Temperature dependence of elastic constants of embedded-atom models of palladium

Ralph J. Wolf, Khalid A. Mansour, and Myung W. Lee
Westinghouse Savannah River Company, Savannah River Technology Center, Aiken, South Carolina 29808

John R. Ray
Department of Physics and Astronomy, Clemson University, Clemson, South Carolina 29634-1911
(Received 3 April 1992)

The elastic constants of fcc palladium are calculated as a function of temperature for four different embedded-atom-method (EAM) models and compared to experimental values. Two of these EAM models have been derived by other workers whereas two of the models are new. Because of the elastic anomaly near 120 K, in the shear constant C_{44} of Pd, the use of this zero-temperature elastic constant to determine the Pd EAM potential leads to errors in the calculated C_{44} above the Debye temperature of 280 K where the potentials are to be used. To correct this behavior we determine the EAM potential in the two new EAM models so that C_{44} is in much better agreement with the experimental value above the Debye temperature. Interestingly in both of these new models the melting temperature is significantly higher and in better agreement with the experimental value of 1825 K. One of our models uses a conventional EAM third-neighbor interaction model whereas our other model is a fifth-neighbor interaction model.

I. INTRODUCTION

The embedded-atom method (EAM) (Ref. 1) of developing interaction potentials is being increasingly used to develop potentials to study material properties. The refinement of the method and its extension to more complex materials is still evolving.[2,3] For background material on the EAM we refer the reader to Refs. 2 and 3, which contain many references to the motivation and development of the theory as well as applications.

In the EAM procedure one normally fits to some material properties at 0 K and then uses the derived potentials in classical simulations at temperatures above the Debye temperature. There has not been a careful study of temperature dependence of properties using EAM potentials. In this paper we present a detailed study of the temperature dependence of several material properties for four different EAM potentials for the element palladium.

We have obtained the EAM potential for Pd determined by Foiles, Baskes, and Daw[4] and another EAM potential for Pd derived by Voter.[5] Along with these two potentials we have also developed two new potentials which incorporate the 120 K elastic anomaly in the shear constant C_{44}. We calculate and present, as a function of temperature, and at zero pressure the elastic constants, linear thermal-expansion coefficient, and isobaric specific heat and compare these to experimental values. We have also obtained an estimate of the thermodynamic melting temperature of each model. The volume versus temperature and energy versus temperature of the four models are also compared. Although there are other important properties besides these we could study, we chose these because they have played an important role in the development of EAM potentials.

To calculate the thermodynamic properties of the models we make use of fluctuation formulas associated with the microcanonical ensemble form of molecular dynamics.[6] This calculational procedure is efficient and takes into account in an exact way the anharmonic contributions to the equilibrium thermodynamic properties. In Sec. II we outline the method used to obtain our two new EAM models of Pd, whereas in Sec. III we give a brief review of the statistical mechanics formulas used for calculating the elastic constants in microcanonical ensemble molecular dynamics. In Sec. IV we present the results of our calculations for the four models and compare with the experimental data, and in Sec. V we shall make some concluding remarks.

II. NEW EAM POTENTIALS FOR Pd

In the EAM the potential energy $E_{\rm pot}$ of the system can be written as a term associated with the energy to embed an atom in the electron density at the atom location and a two-body pair potential which includes the repulsive interaction between two atoms at short distances

$$E_{\rm pot}=\sum_{a=1}^{N} F_a(\rho_a)+\sum_{\substack{a,b=1\\ a<b}} \phi_{ab}(r_{ab})\ , \tag{2.1}$$

where $\phi_{ab}(r_{ab})$ is the two-body interaction potential evaluated at the interatomic distance r_{ab} between atoms a and b, $F_a(\rho_a)$ is the embedding energy of atom a for the electron density ρ_a; ρ_a is the electron density at atom site a due to all other atoms in the system

$$\rho_a=\sum_{\substack{b=1\\ b\neq a}} \rho_b^{\rm at}(r_{ab})\ , \tag{2.2}$$

where ρ^{at} is the atomic (at) electron density. Our method of obtaining the EAM functions follows most closely that of Voter and Chen,[7] and Chen, Srolovitz, and Voter[8] and has also been recently used by Adams and Foiles.[2] The pair term is assumed to be a Morse potential

$$\phi(r)=D(e^{-2\alpha(r-r_0)}-2e^{-\alpha(r-r_0)}) , \quad (2.3)$$

where D is the depth of the minimum located at r_0, and α determines the derivatives of the function (or shape) at the minimum. The three Morse parameters are determined in the empirical EAM fitting procedure. The atomic electron density is given by[7]

$$\rho(r)=r^6(e^{-\beta r}-512e^{-2\beta r}) , \quad (2.4)$$

where β is an adjustable parameter determined in the fitting. This expression for ρ is a modified form of the density of a 4s orbital. The embedding function $F(\rho)$ is found by the Foiles[9] inversion method utilizing the equation of state developed by Rose *et al.*,[10] which states that the energy of a perfect crystal E_{cry} at 0 K and, at a given lattice constant a, is given by

$$E_{cry}(a)=-E_{coh}(1+a^*)e^{-a^*} , \quad (2.5)$$

where E_{coh} is the cohesive energy of the crystal, a^* is defined by

$$a^*=\left[\frac{a}{a_0}-1\right]\left[\frac{9B\Omega}{E_{coh}}\right]^{1/2} , \quad (2.6)$$

and a_0 is the equilibrium lattice constant, B is the 0 K bulk modulus, and Ω is the equilibrium atomic volume. At any given lattice constant a the energy of a single atom in the lattice can be determined by Eq. (2.1) or alternatively by Eq. (2.5). These two energies are required to be the same and the value of the embedding energy F at that energy is determined; a corresponding density given by Eq. (2.2) then defines $F(\rho)$. This digital form of $F(\rho)$, so determined, guarantees that the system behaves according to the Rose *et al.*[10] equation of state at 0 K; it follows that the 0 K lattice constant, cohesive energy, and bulk modulus are exactly reproduced by the model.

In order to perform molecular-dynamics simulations on the system conveniently, we truncated the EAM functions in a "smooth" fashion. To do this we utilized a "shift-force" method where $\phi(r)$ and $\rho(r)$ are cutoff at a distance $r=r_{cut}$ by using

$$f_{smooth}(r)=f(r)-f(r_{cut})+(r_{cut}-r)\left[\frac{df}{dr}\right]_{r=r_{cut}} , \quad (2.7)$$

where $f(r)=\phi(r)$ or $\rho(r)$. For our third- and fifth-neighbor palladium models $r_{cut}=5.4$ Å and 7.4 Å, respectively. This cutoff procedure affects the equation of state if the lattice is expanded to the point where the first-neighbor distance approaches the cutoff distance since then Eq. (2.1) is zero but Eq. (2.5) is nonzero and as a consequence, $F(\rho)$ at $\rho=0$ is nonzero. This problem can be repaired by altering the equation of state, Eq. (2.5) as has been done before, however, we chose not to alter the equation of state; since we have no intention of using these models for free atoms this point has no adverse consequences. Furthermore, the value of the equation of state, and thus $F(0)$ is small at the lattice constant $a=2^{1/2}r_{cut}$, for the third-neighbor model [$F(0)=-0.058$ eV] and still smaller for the fifth-neighbor model (-0.0074 eV).

Our fitting procedure utilizes the equations outlined above along with experimental data to fit D, α, r_0, and β. The experimental data we chose to fit followed that of Adams and Foiles,[2] which is nearly the same as Voter and Chen.[7] We fitted the three elastic constants C_{11}, C_{12}, and C_{44}, the vacancy formation energy ΔE_{1v}^f, but only weakly fitted the dimer properties (bond energy D_e and bond length R_e). As mentioned previously, the experimental C_{44} elastic constant used in the fitting was adjusted to account for an anomaly in its temperature dependence. The 0 K value of 71.2 GPa was increased to 79.5 GPa to shift the C_{44} value to agree with the experimental data in the 300–400 K range. The extent of this shift was determined by observing that the palladium EAM potentials developed by Foiles, Baskes, and Daw[4] and Voter[5] gave significantly low values for C_{44} in molecular-dynamics simulations at elevated temperatures (see Fig. 3), but the two potentials had similar temperature trends. The value of 79.5 GPa was determined by noting that the Voter result is off by approximately 8.3 GPa at 350 K. Shifting the 0 K value of C_{44} by 8.3 GPa should yield an EAM potential for which C_{44} is near the experimental curve near 350 K, which is indeed the case.

A simplex method was used to search the parameters space (D, α, r_0, and β) to minimize the difference between the calculated and the desired properties (C_{11}, C_{12}, C_{44}, ΔE_{1v}^f, D_e, and R_e). The function used to measure the "goodness-of-fit" was defined by

TABLE I. Summary of the EAM fitting procedure for the two new potentials. Note that a_0, E_{coh}, and B are fitted exactly because of our fit to the Rose *et al.* (Ref. 10) equation of state; this is indicated by the square brackets around the values.

Properties	Expt.	Calc. (PDW3)	Calc. (PDW5)
a_0 (Å)	3.89	[3.89]	[3.89]
E_{coh} (eV)	3.91	[3.91]	[3.91]
B (GPa)	195	[195]	[195]
C_{11} (GPa)	234	230	230
C_{12} (GPa)	176	177	179
C_{44} (GPa)	79.5[a]	78.1	80.4
ΔE_{1v}^f (eV)	1.54	1.58	1.48
D_e (eV)	0.70	0.98	0.69
R_e (Å)	2.4	2.53	2.54
Parameters			
D (eV)		1.7778	1.5985
α (Å^{-1})		1.3665	1.4886
r_0 (Å)		2.3323	2.3685
β (Å^{-1})		3.0167	3.0719
r_{cut} (Å)		5.4	6.4

[a]Experimental value is 71.2 GPa.

$$\sum_i \left[\frac{w_i(f_i^c - f_i^d)}{f_i^d} \right]^2 ,$$

where f_i^c is the calculated property, f_i^d is the desired property, and w_i is the weight. The dimer properties were given weights of 0.2; all other weights were unity. The desired values used in the fitting are found in Table I along with all calculated values and the fitted parameter values for the new palladium models which are denoted PDW3 and PDW5 for the third- and fifth-neighbor models, respectively.

III. MOLECULAR-DYNAMICS PROCEDURES AND FORMULAS

In the molecular-dynamics method we solve Newton's laws of motion for the trajectories of the atoms in a many-body simulation. For a general discussion of molecular dynamics we refer the reader to the book by Allen and Tildesley[11] and references contained therein. In the simulations reported on in this paper we have employed 500 Pd atoms initially arranged in an fcc solid. Periodic boundary conditions have been applied in all three dimensions to remove the surface effects of the small system. We used the Gear fifth-order predictor-corrector algorithm[11] with a time step of 2.036×10^{-15} s which is about $\frac{1}{70}$ of the shortest vibrational period in the system. For this algorithm and time step we found accurate energy (enthalpy) and linear momentum conservation in all of the simulations.

The force on atom a, $\mathbf{F}_a$, may be obtained from the potential energy $E_{\rm pot}$ given in Eq. (1):

$$\mathbf{F}_a = -\frac{\partial E_{\rm pot}}{\partial \mathbf{x}_a} , \tag{3.1}$$

which yields

$$\mathbf{F}_a = -\sum_{\substack{b=1 \\ b\neq a}} \left[\frac{\partial F_a}{\partial \rho_a}\frac{\partial \rho_b^{\rm at}}{\partial r_{ab}} + \frac{\partial F_b}{\partial \rho_b}\frac{\partial \rho_a^{\rm at}}{\partial r_{ab}} + \frac{\partial \phi_{ab}(r_{ab})}{\partial_{ab}} \right] \hat{\mathbf{r}}_{ab} , \tag{3.2}$$

where $\hat{\mathbf{r}}$ denotes a unit vector along $\mathbf{r}$. To simplify the notation we shall in the future denote derivatives of $F_a(\rho_a)$, $\rho_a^{\rm at}(r_{ab})$, and $\phi_{ab}(r_{ab})$ with respect to the appropriate argument by a prime. The microscopic stress tensor can be obtained from the virial theorem and has the form

$$P_{ij} = \frac{1}{V}\left[\sum_{a=1}^{N} \frac{p_{ai}p_{aj}}{m_a} - \sum_{\substack{a,b=1 \\ a<b}} (F_a'\rho_b^{\rm at'} + F_b'\rho_a^{\rm at'} + \phi_{ab}')\frac{X_{abi}X_{abj}}{r_{ab}} \right] , \tag{3.3}$$

where V is the volume of the system, p_{ai} is the ith cartesian component of the momentum of particle a, and x_{abi} is the ith component of the relative position vector of particle a and b.

A. Calculational methods

In the present study we used Parrinello-Rahman[12] HtN molecular dynamics to determine the reference values h_0 and V_0 for the pressure $P_{\rm ext}=0$ and tension $t_{\rm ext}=0$. At each temperature in our study we determined the reference values of h and V by carrying out HtN simulations of typically 50 000 iterations or 102 ps after equilibration of the system. We then used these reference values to determine the elastic constants, and other properties using microcanonical or EhN molecular dynamics simulations. Note that in the HtN simulations we also determined the energy-versus-temperature and volume-versus-temperature relations for zero pressure and tension. Although one could, in principle, determine the elastic constants using HtN fluctuation formulas, these formulas are known to be only marginally satisfactory because of slow convergence,[13] however, we did use the scalar fluctuation formulas of HtN ensemble molecular dynamics[13] to check on selected values of the constant pressure specific heat, thermal-expansion coefficient, and adiabatic bulk modulus, which were determined in the EhN ensemble molecular-dynamics simulations. This gives a good check on the EhN calculations.

B. Microcanonical, EhN, molecular dynamics

In microcanonical molecular dynamics we can determine the adiabatic elastic constants (elastic modulii or stiffness coefficients) C_{ijkm} by using fluctuation formulas derived by Ray and Rahman[6] and shown to be efficient by Ray, Moody, and Rahman[14]:

$$C_{ijkm} = -\frac{V_0}{k_B T}(\langle P_{ij}P_{km}\rangle - \langle P_{ij}\rangle\langle P_{km}\rangle) + \frac{2Nk_BT}{V_0}(\delta_{ik}\delta_{jm}+\delta_{im}\delta_{jk}) + \langle B1_{ijkm}\rangle + \langle B2_{ijkm}\rangle + \langle B3_{ijkm}\rangle , \tag{3.4}$$

where the three Born terms have the form

$$B1_{ijkm} = \frac{1}{V_0}\sum_{\substack{a,b=1 \\ a<b}} \left[\phi_{ab}'' - \frac{\phi_{ab}'}{r_{ab}} \right] \frac{x_{abi}x_{abj}x_{abk}x_{abm}}{r_{ab}^2} , \tag{3.5}$$

$$B2_{ijkm} = \frac{1}{V_0}\sum_{\substack{a,b=1 \\ a\neq b}} F_a' \left[\rho_b^{\rm at''} - \frac{\rho_b^{\rm at'}}{r_{ab}} \right] \frac{x_{abi}x_{abj}x_{abk}x_{abm}}{r_{ab}^2} , \tag{3.6}$$

$$B3_{ijkm} = \frac{1}{V_0}\sum_{a=1}^{N} F_a'' g_{aij}g_{akm} , \tag{3.7}$$

and g_{aij} is given by

$$g_{aij} = \sum_{\substack{b=1 \\ b\neq a}} \frac{\rho_b^{\rm at'}x_{abi}x_{abj}}{r_{ab}} . \tag{3.8}$$

The first term in Eq. (3.4) is called the fluctuation term, while the second term is called temperature correction term. Later we shall give specific values for these

different contributions to the elastic constants for selected cases.

Fluctuations in the kinetic energy K in the EhN ensemble give the specific heat at constant volume C_V:

$$\langle K^2\rangle-\langle K\rangle^2=\frac{3N}{2}\left[1-\frac{2Nk_B}{2C_V}\right], \tag{3.9}$$

whereas the cross fluctuation between the kinetic energy and the microscopic pressure function $P=\frac{1}{3}\sum p_{ii}$ allows one to obtain the linear thermal-expansion coefficient α of the system

$$\langle PK\rangle-\langle P\rangle\langle K\rangle=(k_BT)^2\frac{N}{V_0}\left[1-\frac{9\alpha B_TV_0}{2C_V}\right], \tag{3.10}$$

where B_T is the isothermal bulk modulus. The adiabatic bulk modulus can be obtained from the elastic constants by $B_S=(C_{11}+2C_{12})/3$, since the pressure and tension are zero. Using standard thermodynamic relationships we can obtain the specific heat at constant pressure C_p and determine explicitly the linear thermal-expansion coefficient α.

In summary our calculational procedure consists of the following steps: At each temperature we determined a reference value of h, h_0 by calculating the average value of h in an HtN molecular-dynamics simulation. Next we carried out an EhN molecular-dynamics simulation with $h=h_0$ and employed the above fluctuation formulas, to determine the elastic constants, the specific heat at constant pressure, and the linear thermal-expansion coefficient for each of the four model potentials at several temperatures. For the averages in the EhN simulations we typically ran 50 000 iterations or 102 ps for each temperature and, of course, each potential, and often we followed this by another 50 000 iterations to check on the convergence of the results. For selected runs we ran longer to check on convergence.

As discussed by Johnson,[15] there is a type of "gauge invariance" of $E_{\rm pot}$ defined by the transformation

$$F_a(\rho)\rightarrow F_a(\rho)+c_a\rho,\quad \phi_{ab}\rightarrow\phi_{ab}-c_a\rho_b^{\rm at}-c_b\rho_a^{\rm at}, \tag{3.11}$$

where c_a is an arbitrary constant. Under this transformation, the two Born terms $B1$ and $B2$ are modified, but their sum remains invariant, however, the $B3$ term, which is related to the curvature of the embedding function, is invariant under this transformation. Notice that the $B1$ and $B2$ terms are pair terms and the entire many-body contribution of the EAM potential to the elastic constants is contained in the $B3$ term, which is also the term that breaks the 0 K Cauchy relation $C_{12}=C_{44}$. The fluctuation term and the temperature correction term break the Cauchy relation at finite temperature. Thus, if we are using EAM potentials that differ only by a gauge transformation from one another, the term $B3$ will be the same for both potentials. A comparison of the $B3$ terms at 0 K, therefore, gives a simple way of telling whether the two potentials could be related by a gauge transformation.

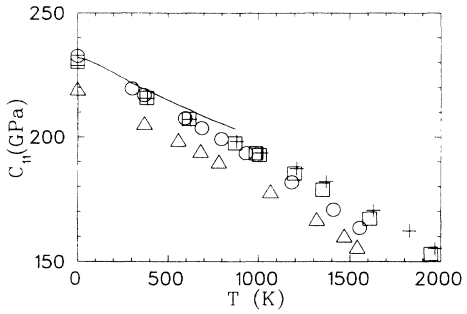

FIG. 1. C_{11} vs temperature for four models of Pd and the experimental data from Ref. 16. The line represents the experimental data whereas the symbols show the simulation points; the triangle is for the FBD potential, the circle is for the VOT potential, the box is for the PDW3 potential, and the plus sign is for the PDW5 potentials.

IV. RESULTS

1. Elastic constants

In Figs. 1, 2, and 3 we show the elastic constants C_{11}, C_{12}, and C_{44} as a function of temperature obtained with the four model potentials as well as the experimental elastic constant data as reported in the Landolt-Bornstein compilation,[16] which is shown by the solid line. The Landolt-Bornstein data for Pd at temperatures below 300 K is consistent with the more recent experimental data given by Nygren and Leisure.[17] The experimental data is only available to 900 K. In order to refer to the potentials individually we refer to the Foiles, Baskes, and Daw[4] potential as FBD, denoted by △ in the figures, the Voter[5] potential as VOT, denoted by ○ in the figures, the new third-neighbor potential as PDW3, denoted by □ in the figures, and the new fifth-neighbor potential as PDW5, denoted by + in the figures. Our inclusion of the fifth-neighbor model is mainly to check in a quantitative way the difference between a third-neighbor model and a fifth-neighbor model. EAM applications have almost universally used a third-neighbor or less model with no quantitative comparison of finite temperature properties between the two different types of models.

For C_{11} all four potentials show nearly the correct decrease with temperature until after 500 K, where the experimental values do not show as much softening as the

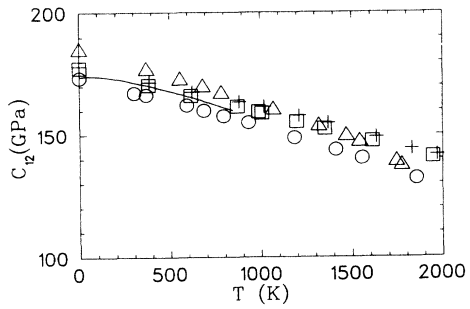

FIG. 2. C_{12} vs temperature. The symbols have the same meaning as in Fig. 1.

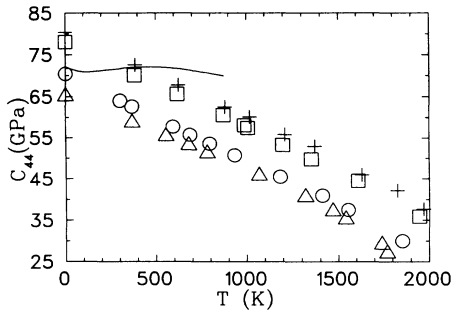

FIG. 3. C_{44} vs temperature. The symbols have the same meaning as in Fig. 1.

models. Note that FBD was not fitted as accurately to the 0 K elastic constants as the other models, so it looks worse in this comparison. By carrying out independent simulations we obtain independent determinations of the elastic constants and can use these to estimate the computational errors in these quantities. In all cases we estimate the errors in the elastic constants to be less than 1%. This error is expected due to the small value of the fluctuation term in Eq. (3.4) which controls the error in the calculation.[13]

For C_{12} we again see good agreement between experiment and the models over the entire temperature range, especially so for the two new models. Note that, from the point of view of the elastic constants, the two new models PDW3 and PDW5 give essentially the same results, except at higher temperatures where PDW3 is seen to soften more than PDW5.

For C_{44} we do not find as good an agreement between the models and experiment mainly because of the 120 K anomaly in C_{44}. This anomaly is interpreted by Rayne[18] to be associated with the change with temperature of the contribution by the holes in the 4*d* band in Pd. The EAM potentials cannot, at this stage of their development, explain such a subtle electronic structure property. As mentioned in Sec. II for PDW3 and PDW5, we have fitted to a higher value of C_{44} at 0 K so that near room temperature the calculated elastic constant is close to the experimental value. Since our classical simulations are valid only above the Debye temperature, of 280 K for Pd, the mechanical properties of PDW3 and PDW5 should be better than the other two potentials at temperatures where classical simulations are valid. Basically what we are doing is determining the EAM potential by fitting to a finite temperature property instead of a zero-temperature property; since the EAM is empirical, at the present time, our approach seems to be a preferable way of developing the EAM potential for Pd. For higher temperatures even the two new models show significant deviations from the experimental values for C_{44}. The slope of the simulation values for C_{44} in Fig. 3 shows considerable deviation from the experimental values. This discrepancy is probably also due to the elastic anomaly since at higher temperatures C_{44} would be expected to soften more rapidly; the elastic anomaly delays the softening of C_{44} until higher temperatures and this gives rise to the difference in slopes of the theoretical and experimental values in Fig. 3.

TABLE II. The zero-temperature elastic constants for the four models broken down into the different terms in Eq. (3.4). The elastic constants are given in units of GPa.

	C_{11}	C_{12}	C_{44}
	FBD $T=0$ K		
$B1+B2$	98.99	65.07	65.07
$B3$	119.54	119.54	0.0
Total	218.53	184.61	65.07
	VOT $T=0$ K		
$B1+B2$	129.59	70.36	70.36
$B3$	102.99	102.99	0.0
Total	232.58	173.35	70.36
	PDW3 $T=0$ K		
$B1+B2$	130.81	78.07	78.07
$B3$	99.37	99.37	0.0
Total	230.18	177.44	78.07
	PDW5 $T=0$ K		
$B1+B2$	130.81	80.36	80.36
$B3$	97.88	97.88	0.0
Total	228.69	178.24	80.36

In Table II we give the Born terms at 0 K for all four models and the elastic constants as determined from Eq. (3.4). Table II shows that both Born terms give significant contributions, with the many-body Born term, $B3$, being around 100 GPa for the last three potentials. Recall that the two-body Born terms do not have a gauge invariant significance by themselves and only the sum is gauge invariant, thus we give only the sum $B1+B2$ in Table II. Note that the many-body term does not contribute to C_{44}, which clearly shows the breaking of the Cauchy relation at 0 K. At elevated temperatures each of the Born terms decreases in absolute magnitude, due to the increase in volume and to the averaging associated

TABLE III. The elastic constants for the potential PDW3 at two temperatures broken down into the different terms in Eq. (3.4). The elastic constants are given in units of GPa.

	C_{11}	C_{12}	C_{44}
	PDW3 $T=382.8$ K		
Fluct	−6.38	−0.14	−4.40
T Corr	1.42	0.0	0.71
$B1+B2$	123.58	73.73	73.73
$B3$	97.45	97.45	0.02
Total	216.07	171.00	70.06
	PDW3 $T=1007.2$ K		
Fluct	−18.28	−1.47	−11.88
T Corr	3.64	0.0	1.82
$B1+B2$	113.36	67.07	67.07
$B3$	93.93	93.82	0.0
Total	192.65	159.42	57.07

with the increase in size of the Debye-Waller thermal cloud. Also, the fluctuation term is nonzero and increases with temperature whereas the temperature correction term in Eq. (3.4) becomes nonzero.

As an illustration of these trends we show in Table III the contributions to the elastic constants for PDW3 for two different temperatures, 383 K and 1007 K. The other models show this same general type of behavior as the temperature is raised. Note in particular the growth in importance of the fluctuation term with temperature from 3% at 383 K to 9.5% at 1007 K for C_{11}. Thus, the fluctuation term plays an increasing role in the softening at elevated temperatures. At a temperature of 2100 K, where the model PDW3 is superheated and near the point of mechanical instability of the crystal, the fluctuation term is 44% of the elastic constant C_{11}.

2. Thermal expansion

In Fig. 4 we show the linear thermal-expansion coefficient calculated for the four models using Eqs. (3.4), (3.9), and (3.10) along with experimental data.[19] Although all four models show the same general increase as the experimental values, they are on average lower than the experimental data. In order to check the convergence of the values obtained, we continued some averaging runs for 200 000 iterations, and found only small changes in the values; not enough to change the graphs in Fig. 4. We also carried out HtN calculations of the thermal-expansion coefficient using fluctuation formulas appropriate to that ensemble.[13] As examples for PDW3 at 872 K we found $\alpha_{\mathrm{HtN}}=12.04\times10^{-6}$ K^{-1} and $\alpha_{\mathrm{EhN}}=12.9\times10^{-6}$ K^{-1}, while in another calculation at 987 K we found $\alpha_{\mathrm{HtN}}=12.8\times10^{-6}$ K^{-1} and $\alpha_{\mathrm{EhN}}=13.1\times10^{-6}$ K^{-1}. Although these are not the same values they would not change the character of the simulation results shown in Fig. 4. As an alternate method we determined α by numerically differentiating the V versus T zero pressure isobar. This gives a curve that is essentially a fit of the data in Fig. 4 by a smooth curve. The fluctuation expressions are an analytical expression of this derivative and, therefore, both methods should and do give the same results. Since we were calculating the elastic constants by the fluctuation formulas, the calculation of α in the same simulation does not use any more computer time. Our results for the linear thermal-expansion coefficient for the FBD potential agree with the single room-temperature value given for this potential by Foiles and Daw,[20] namely $\alpha=10.9\times10^{-6}$ K^{-1}. We consider the calculated linear thermal expansion to be satisfactory for all four models.

3. Specific heat

In Fig. 5 we show the dimensionless, constant pressure specific heat per particle as determined by the fluctuation formulas compared to experimental values.[21] Again all four models show the observed increase of C_p with temperature. We again checked selected values of C_p by using HtN fluctuation formulas which were consistent with the results in Fig. 5. We also numerically differentiated the E versus T zero pressure isobar to check the specific heat values. Note the two high-temperature points with C_p near 4.9 in Fig. 5. These points are near the temperature of the mechanical instability for these two potentials; the larger values given by the fluctuation formula are a precursor of the incipient phase transformation. Since the two new potentials become mechanically unstable at higher temperatures, the fluctuation formulas still give reasonable results for these potentials at these temperatures. Again we consider the agreement of the calculated specific heat to be satisfactory for all the models.

4. Melting

Palladium melts at a temperature of 1825 K. The thermodynamic melting temperature (temperature for equality of free energies of solid and liquid phases) is difficult to directly determine accurately for a small system with three-dimensional periodic boundary conditions because of the ability of the system to be superheated far above the melting temperature. In order to estimate the thermodynamic melting temperature, we used the method introduced by Kluge, Ray, and Rahman.[22] In this method one raises the temperature of the system slowly until it becomes mechanically unstable; the system then melts and cools. The final temperature of the melt is an upper bound on the thermodynamic melting temperature since the system has undergone a phase transformation to a more stable phase, namely the liquid phase at the final temperature. Kluge, Ray, and Rahman found this

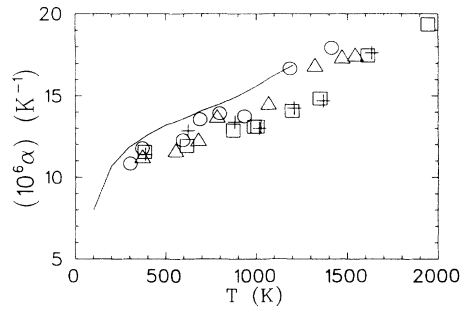

FIG. 4. Linear thermal-expansion coefficient for the four models compared to experimental values from Ref. 19. The symbols have the same meaning as in Fig. 1.

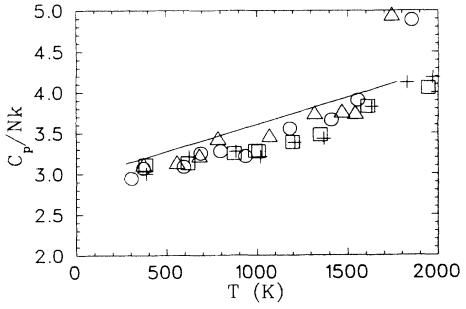

FIG. 5. Dimensionless specific heat for the four models compared to experimental values from Ref. 21. The symbols have the same meaning as in Fig. 1.

method to give a temperature about 5% higher for silicon than the thermodynamic melting temperature as determined by more involved free-energy methods. Foiles and Adams[23] used a free-energy method to determine the melting temperatures. This method is considerably more involved than the present method and also subject to its own numerical errors. A more accurate way of estimating the thermodynamic melting temperature is to introduce a free surface and determine the interface velocity as a function of temperature. By interpolating the interface velocity to zero we may determine the melting temperature.[24] For the present purposes our simpler method, which has been shown to give results to within 5% of the correct value, is satisfactory. In Table IV we show our results for the melting of the four models of Pd along with the previous estimates by other workers for the FBD (Ref. 23) and VOT (Ref. 25) potentials. We find similarly to Wolf, Okamoto, Yip, Lutsko, and Kluge[26] that as the superheated fcc crystal becomes unstable and disorganizes the minimum shear modulus $(C_{11}-C_{12})/2$ goes to zero. In Fig. 6 we show the minimum shear modulus as determined in the simulations as well as the experimental values. The low melting point of the FBD potential is probably due to the fact that the O K fit to the minimum shear modulus is too low as can be seen in Fig. 6. Note that the final approach of the minimum shear modulus to zero is not linear for any of the potentials; this can be seen for the FBD and VOT potentials in Fig. 6. The two new potentials have higher melting temperatures than the earlier models. As mentioned previously; the main difference in the determination of the two new potentials is to take into account the C_{44} shear anomaly. The value of the shear modulus $(C_{11}-C_{12})/2$ is still fitted to the experimental values for the new potentials as is shown in Fig. 6. Note that the VOT potential actually fits a higher value of the minimum shear modulus but melts at a lower temperature than the two new models. It is also interesting that PDW5 melts at a higher temperature than PDW3, which is what one would expect since extending the potential to more neighbors should increase the stability of the crystal because these more distant neighbors are in the attractive part of the potential. Our estimate of the melting temperature of PDW5 is 1828 K compared to the experimental value of 1825 K. The FBD and VOT potentials both melt at too low a temperature.

TABLE IV. The mechanical instability temperatures and estimated melting temperatures of the four models of Pd. The first two columns are results of this study. The last column is from previous studies.

Potential	Instability temperature (K)	Melting temperature (K)	Melting temperature (K)
FBD	1800	1480	1390[a]
VOT	1950	1588	1520±150[b]
PDW3	2200	1728	NA
PDW5	2300	1828	NA

[a]Reference 23.
[b]Reference 25.

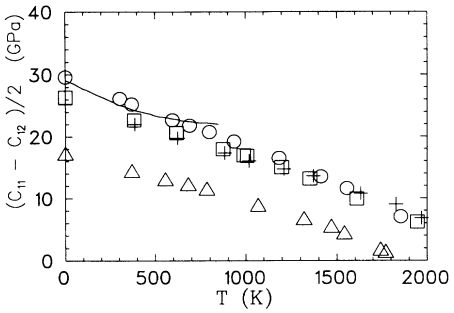

FIG. 6. Minimum shear modulus vs temperature for the four models compared to experimental values. The symbols have the same meaning as in Fig. 1.

By subtracting the enthalpy of the solid from the liquid at the estimated melting temperatures, we obtain an estimate of the latent heat of the phase transformation. These results for the four potentials are shown in Table V, along with the density of the liquid at the estimated melting temperatures determined in the simulations. Table V also contains the experimental latent heat and liquid density.[27] The latent heat is low for all four models, while the density of the liquid is in satisfactory agreement with the observed value. We do not have an explanation of why the latent heat is low for the EAM models, although it is interesting that Kluge, Ray, and Rahman[22] found that the melting point was reasonable for silicon but the latent heat was only half the observed value. The calculation of the latent heat using traditional condensed matter theory is a difficult problem due to the fact that this is a highly nonequilibrium process.

5. *Energy and volume versus temperature*

In Figs. 7 and 8 we show the energy (enthalpy) and volume versus temperature for the four models. Note the liquid phase points above the solid phase points in the high-temperature part of these figures. The lowest temperature liquid point shown in Figs. 7 and 8 for each of the potentials gives our upper bound estimate of the melting temperature. In general, the volume and energy of the four models behave in a similar fashion as a function of temperature except at the highest temperatures where the FBD and VOT potentials are close to becoming unstable.

TABLE V. The latent heat and liquid density at the melting temperature for the four models of Pd along with experimental values from Ref. 27.

Potential	Liquid density (g/cm^3)	Latent heat (kJ/mol)
FBD	10.97	7.79
VOT	10.81	9.96
PDW3	10.81	10.2
PDW5	10.72	9.84
Expt.[a]	10.5	16.7

[a]Reference 27.

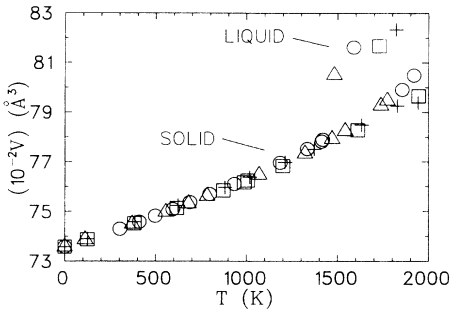

FIG. 7. Volume vs temperature for the four model potentials. This is the zero pressure zero tension volume for the 500-particle system. The symbols have the same meaning as in Fig. 1.

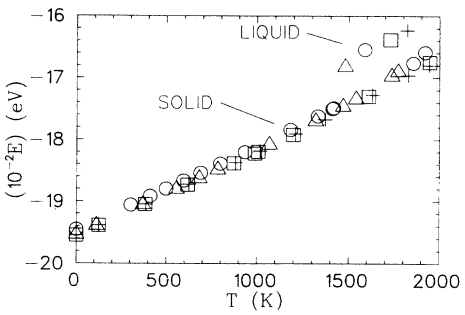

FIG. 8. Energy (enthalpy) vs temperature for the four model potentials. The symbols have the same meaning as in Fig. 1.

V. SUMMARY AND CONCLUSIONS

We have given a detailed and quantitative comparison of four EAM potentials for the element palladium from the point of view of the temperature dependence of selected thermodynamic properties as well as the melting properties of the models. Due to the fact that Pd has an elastic anomaly in C_{44} we have modified the EAM procedure and fit to a higher value of this property so that the calculated value in the temperature range 300–400 K is close to the experimental values. One of the new models, PDW3, is a third-neighbor model, whereas, the other model, PDW5, is a fifth-neighbor model. Because we have taken the elastic anomaly into account, the mechanical properties of the two new model potentials should be better than the previous models in the temperature range of most interest, 300–400 K.

Most EAM models have been third-neighbor or less models and we constructed the fifth-neighbor model to test whether including more neighbors would change the temperature dependence of thermodynamic properties in an important way. From a study of Figs. 1–8 we conclude that it is sufficient to consider only third-neighbor models for this system. The difference between PDW3 and PDW5 is probably not significant from the point of view of modeling within the current EAM scheme, although the two models do have different melting temperatures because of the more rapid softening of the elastic constants of PDW3 at elevated temperatures. It is possible that the melting temperature of PDW3 could be elevated by increasing the calculated value of C_{44} in Table I, but we did not explore this possibility. By studying the exponential falloff of the electron density one would suspect that the third- and fifth-neighbor models would have similar properties and this is indeed the case. The two new models are more similar to each other than to the previous models and are more like the VOT potential than the FBD potential.

In all models the melting of the crystal takes place by an elastic instability in the minimum shear modulus which ultimately approaches zero in the superheated crystal. Upper limits on the melting temperatures were determined by slowly heating the crystal to the point of mechanical instability and then allowing the melt to cool to a final temperature which is an upper bound on the thermodynamic melting temperature. The two new models have melting temperatures in better agreement with experiment.

The linear thermal-expansion coefficient and the specific heat at constant pressure of the four models show satisfactory agreement with experiment as the temperature is elevated. In summary, we have presented two new EAM models for palladium and given a quantitative comparison of finite temperature thermodynamic properties calculated by molecular dynamics, which contain all anharmonic effects. The two new models have better mechanical properties than the previous models and have melting temperatures nearer the correct value.

ACKNOWLEDGMENTS

We acknowledge support from the U.S. Department of Energy under Contract No. DE-AC09-88SR18035 and through SCUREF. We thank Dr. S. Foiles for supplying the FBD potential and Dr. A. Voter for supplying the VOT potential. We also thank R. Davis, S. Foiles, T. Graham, R. Leisure, and A. Voter for helpful discussions.

[1]M. S. Daw and M. I. Baskes, Phys. Rev. Lett. **50**, 1285 (1983); Phys. Rev. B **29**, 6443 (1984).

[2]J. B. Adams and S. M. Foiles, Phys. Rev. B **41**, 3316 (1990).

[3]S. P. Chen, A. F. Voter, R. C. Albers, A. M. Boring, and P. J. Hay, J. Mater. Res. **5**, 955 (1990).

[4]S. M. Foiles, M. I. Baskes, and M. S. Daw, Phys. Rev. B **33**, 7983 (1986).

[5]A. F. Voter (private communication).

[6]J. R. Ray and A. Rahman, J. Chem. Phys. **80**, 4423 (1984).

[7]S. P. Chen, A. F. Voter, and D. J. Srolovitz, in *Characterization of Defects in Materials,* edited by R. W. Siegel, R. Sinclair, and J. R. Weertman (Materials Research Society, Pittsburgh, 1987), Vol. 82, p. 175.

[8]S. P. Chen, S. J. Srolovitz, and A. F. Voter, J. Mater. Res. **4**, 62 (1989).

[9]S. M. Foiles, Phys. Rev. B **32**, 7685 (1985).

[10]J. H. Rose, J. R. Smith, F. Guinea, and J. Ferrante, Phys. Rev. B **29**, 2963 (1984).

[11]M. P. Allen and D. J. Tildesley, *Computer Simulation of Liquids* (Oxford University Press, Oxford, 1987).
[12]M. Parrinello and A. Rahman, Phys. Rev. Lett. **45**, 1196 (1980); J. Appl. Phys. **52**, 7182 (1981).
[13]J. R. Ray, Comp. Phys. Rep. **8**, 109 (1988).
[14]J. R. Ray, M. C. Moody, and A. Rahman, Phys. Rev. B **32**, 733 (1985).
[15]R. A. Johnson, Phys. Rev. B **37**, 3924 (1988).
[16]R. F. S. Hearmon, in *Landolt-Bornstein: Crystal and Solid State Physics,* edited by K.-H. Hellweg (Springer-Verlag, Berlin, 1979), Vol. II.
[17]L. A. Nygren and R. G. Leisure, Phys. Rev. B **37**, 6482 (1988).
[18]J. A. Rayne, Phys. Rev. **118**, 1545 (1960).
[19]Y. S. Touloukian, R. K. Kirby, R. E. Taylor, and P. D. Desai, *Thermophysical Properties of Matter: Thermal Expansion of Metallic Elements and Alloys* (Plenum, New York, 1975), Vol. 12.
[20]S. M. Foiles and M. S. Daw, Phys. Rev. B **38**, 12 643 (1988).
[21]Y. S. Touloukian, R. K. Kirby, and R. E. Taylor, *Thermophysical Properties of Matter: Specific Heat of Metallic Elements and Alloys* (Plenum, New York, 1975), Vol. 4.
[22]M. D. Kluge, J. R. Ray, and A. Rahman, J. Chem. Phys. **87**, 2336 (1987).
[23]S. M. Foiles and J. B. Adams, Phys. Rev. B **40**, 5909 (1989).
[24]C. J. Tymczak and J. R. Ray, Phys. Rev. Lett. **64**, 1278 (1990).
[25]F. Ercolessi and A. F. Voter (private communication).
[26]D. Wolf, P. R. Okamoto, S. Yip, J. F. Lutsko, and M. Kluge, J. Mater. Res. **5**, 286 (1990).
[27]T. Iida and R. I. L. Guthrie, *The Physical Properties of Liquid Metals* (Oxford University Press, Oxford, 1988).